AIAA Propulsion and Energy Forum
19-22 August 2019, Indianapolis, IN
AIAA Propulsion and Energy 2019 Forum

10.2514/6.2019-3867

Spray Flamelet Modeling of Kerosene Spray Combustion

Ran Yi,[1] Xu Zhang[1], Tao Yang[1] and C. P. Chen[2]
University of Michigan-Shanghai Jiao Tong University Joint Institute

Shanghai Jiao Tong University, Shanghai, 200240, China,

A spray-based counterflow flame can be modeled as a low-dimensional configuration to reflect the multi-combustion regimes in the realistic liquid-fueled combustion process. This paper firstly presents the spray flame structure with a four-component Jet-A surrogate and ethanol fuels in a counterflow configuration. A double-flame structure exists in the spray diffusion flame and corresponds to the two locations with stoichiometric mixture fraction due to the fuel evaporation. This evaporation effect results in non-monotonicity of the mixture fraction for the spray Flamelet Generated Manifold (FGM) tabulation and causes difficulty in coupling with CFD. Thus, a gaseous FGM table, with the mixture fraction and progress variable as controlling variables, was implemented into the OpenFOAM CFD solver to perform piloted dilute turbulent spray combustion simulations using Jet-A surrogate and ethanol fuels. The SMD distributions are in good agreement with the experimental data, while the temperature field is over-predicted. Further investigation utilizing a two-dimensional counterflow spray flame indicated adding the absolute enthalpy as another manifold in the gaseous FGM table is capable of capturing the non-adiabatic process of the droplet evaporation. Future directions in utilizing the spray flamelet are discussed.

I. Nomenclature

D	=	fuel nozzle diameter
j_k	=	diffusive mass flux of species k
h_k	=	enthalpy of species k
S_ρ	=	evaporation source
S_h	=	heat transfer rate from the liquid phase
S_{Y_k}	=	mass transfer source term of species k
$\tilde{S}_Z$	=	Favre-averaged source term due to evaporation for mixture fraction
u	=	axial velocity
V	=	scaled radial velocity
W_k	=	molecular weight of species k
x	=	axial coordinate
Y_C	=	progress variable
Z	=	mixture fraction
$\tilde{\phi}$	=	Favre-averaged scalar
$\dot{\omega}_k$	=	molar production rate of species k
$\dot{\omega}_{Y_C}$	=	progress variable source term
$\tilde{\chi}$	=	Favre-averaged scalar dissipation rate

[1] Graduate student.
[2] Chair Professor and Associate Dean, AIAA Associate Fellow, chienpin.chen@sjtu.edu.cn

II. Introduction

In a liquid-fueled combustor, the combustion phenomenon is closely linked to the fuel heating, evaporating spray and the subsequent oxidation processes. The spray flame involves non-premixed, premixed and evaporation-controlled combustion regimes and thus forms various multi-regime flame structures. This process is further complicated by the real kerosene fuels, typically composed of thousands of different kinds of hydrocarbon species with different physical properties. Surrogate fuels are required to model real kerosene fuels. In our previous study [1], a four-component Jet-A surrogate fuel was successfully implemented to predict the ignition time delays and lift-off length of the Jet-A in a constant volume combustion chamber. Even the results were promising in Ref. [1], the computational cost is still excessive, especially coupled with the Large Eddy Simulation (LES) methodology.

Flamelet-based combustion models offer a cost-effective way to account for detailed chemical kinetics in realistic turbulent combustion systems. The flamelet approach can be combined with the intrinsic low-dimensional manifold concept by mapping detailed chemical process to a low-dimensional Flamelet-Generated Manifold (FGM). Pierce and Moin [2] adopted an indirect mapping approach, whereby detailed chemical processes were mapped to a reduced system of tracking scalars. The unsteady lifted flame dynamics of a turbulent jet diffusion flame was successfully captured. However, these achievements were made in the context of gaseous combustion while most engineering combustion systems utilized liquid fuel spray combustion. Indeed, it has already been found out that the application of gaseous diffusion flamelet approach to spray combustion leads to noticeable errors [3, 4]. This deviation is likely to be related to the intrinsic physical change after the spray is incorporated into the gaseous diffusion flame. Due to the droplet evaporation process in spray combustion, the mixture fraction does not vary from 0 to 1 as in gaseous diffusion flame. Instead, the mixture fraction increases continuously in the evaporation zone and fuel-air mixture emerges where combustion has already taken place. It leads to a partially-premixed regime in realistic spray combustion. Unlike the diffusion-limited combustion, premixed combustion usually occurs in a fast and intense way. This suggests the need for an improved method especially for spray combustion that is able to account for different combustion regimes. Therefore, using a spray flame library, which was originally proposed by Hollmann and Gutheil [5], is a promising approach to account for multi-regime combustion simulation. However, due to the liquid fuel evaporation, the mixture fraction no longer varies monotonically, which causes some ambiguity in constructing look-up tables. Moreover, a typical spray flame library would utilize extra parameters related to spray characteristics. To overcome this difficulty, some researchers have turned their attention back to the gaseous flamelet model, while adding another controlling variable (e.g. enthalpy) to capture the heat losses associated with the spray evaporation process. Such an idea has been applied in many works [6-8] in which the experimental data of the Sydney spray burner [9] was used for validation.

In the present work, the spray flame structure in a counterflow configuration with Jet-A surrogate and ethanol fuel injection is firstly investigated, to uncover the intrinsic differences among the spray flame FGM's and the gaseous diffusion flame FGM. The issues related to the non-monotonicity when building the spray flamelet look-up tables are investigated. Coupling of an FGM table (gas phases) with a CFD solver has been implemented into the OpenFOAM CFD code to validate its feasibility for a piloted burner configuration using the experimental data of Ref. [9]. Further investigation of the performance of the spray flamelet FGM approach against numerical simulation results using direct integration of chemistry is performed and discussed.

III. Spray Flamelet Analysis

In this section, a laminar spray flamelet model is analyzed, with the main motivation to uncover the inherent characteristics in spray diffusion flame when compared with the gaseous diffusion flame.

A. Counterflow configuration

The counterflow flame, the most widely used configuration in generating the low-dimensional manifold, is the target in this study because it can be simplified to a 1-D problem due to axi-symmetry [10]. In this section, spray flames is directly used to build the low dimensional manifold that can intrinsically cover multiple combustion regimes encountered in realistic spray combustion. In contrast to the non-adiabatic gas-phase FGM approach in which the evaporative cooling effect is accounted for by modifying the inlet enthalpy levels [11], this two-phase flamelet approach is believed to be more representative for describing a realist spray combustion process. The sketch of the counterflow spray flame configuration is shown in Fig. 1.

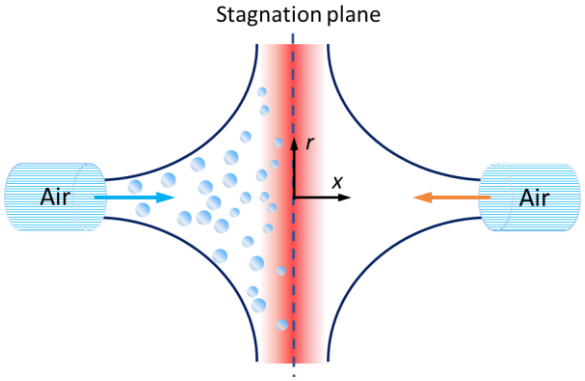

Fig. 1 Sketch of the counterflow spray flame. The spray is injected from the left side.

B. Governing equations and numerical methods

The axisymmetric counterflow configuration, along with Lagrangian particle tracking, has been solved in the framework of the open-source suite Cantera [12]. Heat and mass transfer between gas and liquid phase are two-way coupled, and non-unity Lewis number is considered. Under laminar assumptions, the set of one-dimensional governing equations for gas phase is cast into cylindrical coordinates as follows:

$$\left.\begin{aligned}
&\frac{d(\rho u)}{dx}+2\rho V=S_\rho \\
&\rho\frac{dV}{dt}+\rho u\frac{dV}{dx}+\rho V^2=-\frac{1}{r}\frac{dp}{dr}+\frac{d}{dx}\left(\mu\frac{dV}{dx}\right) \\
&\rho c_p\frac{dT}{dt}+\rho c_p u\frac{dT}{dx}=\frac{d}{dx}\left(\lambda\frac{dT}{dx}\right)-\sum_k j_k c_{p,k}\frac{dT}{dx}-\sum_k h_k W_k\dot{\omega}_k+S_h \\
&\rho\frac{dY_k}{dt}+\rho u\frac{dY_k}{dx}=-\frac{dj_k}{dx}+W_k\dot{\omega}_k+S_{Y_k}
\end{aligned}\right\}, \tag{1}$$

After the solution in physical space, all thermo-chemical variables are then mapped into the mixture fraction space. Here, the mixture fraction is calculated from the element mass fraction of argon.

These partial differential equations are discretized in physical space using the finite-difference method. An efficient hybrid Newton/pseudo-time-stepping method is used to solve the discretized equations. Gird independence is ensured using an adaptive grid. Upwind and central differencing schemes are applied for the convection and diffusion terms respectively. Additional source terms from the liquid phase, namely heat and mass transfer rate terms, are computed in the Lagrangian framework using the second-order Runge-Kutta method for time advancement. Following the work of Miller et al. [13], the non-equilibrium Langmuir-Knudsen law based on infinite liquid conductivity is implemented. To investigate the characteristics of the spray flame, both multi-component Jet-A surrogate and single-component ethanol were chosen as the target fuels. As to the chemical kinetics, the skeleton reaction mechanism POLIMI_231 [14], consisted of 231 species and 5591 reactions, was applied for Jet-A surrogate fuel developed by our previous work [15], and the mechanism containing 31 species and 66 reactions [16] was used for ethanol. For the initial boundary conditions of the counterflow, the left side is the mixture of air and droplets (100μm), while the right side is air, both of which are in temperature of 800 K.

C. Results and discussion for spray counterflow combustion of Jet-A and ethanol

The flame structures of gaseous and spray diffusion flames of Jet-A at the strain rate $a=100\,\mathrm{s}^{-1}$ are shown in Fig. 2 a) and 2 b), respectively. When spray was included, the comparison of the two solutions for Jet-A clearly illustrates the double-flame structure that appears in the spray counter-flow flame. Both the two flames are found corresponding to the vicinity of the stoichiometric mixture fraction 0.068. This suggests a diffusion-controlled regime for both flames, similar to the gaseous case. For ethanol spray flame in Fig. 2 c), the maximum mixture

fraction coincides with the stoichiometric mixture fraction 0.1. Therefore, the double-flame structure merges into one.

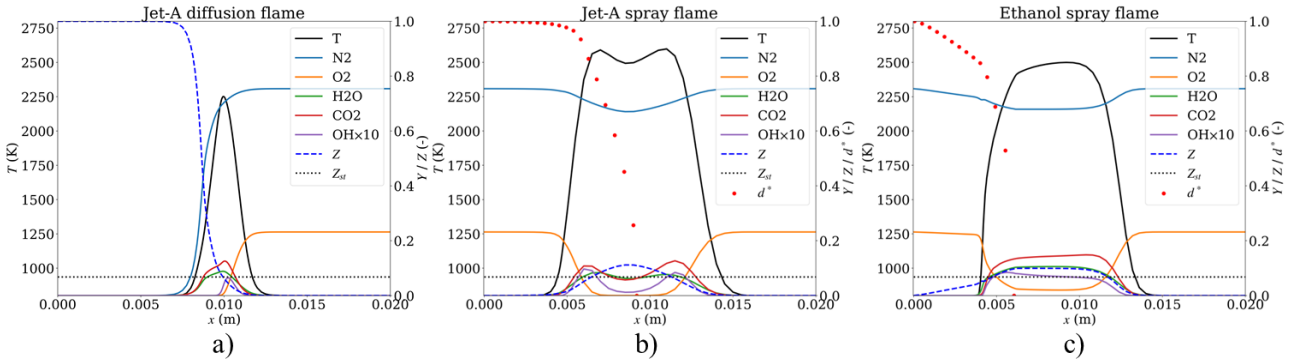

Fig. 2 Counterflow flame structures under the conditions of a=100 s^{-1} and fuel/air inlet equivalence ratio ϕ=1. a) Jet-A gaseous diffusion flame, b) Jet-A spray flame and c) ethanol spray flame. d^* denotes the normalized droplet diameter.

Depending on the inlet conditions, the partially-premixed flame may occur. In the spray flame case Fig. 2 b), the first peak of the temperature profile corresponds to the simultaneous consumption of fuel and oxygen and the combustion products appear after the flame front, which indicates a premixed combustion regime. The second peak of the temperature profile corresponds to the diffusion flame where the right-side air reacts with intermediate products from the left side.

When the liquid fuel evaporates into the gas flow, the mixture fraction no longer varies monotonically (shown in Fig. 2). As a consequence, after mapping into the mixture fraction space, temperature (or other chemical variables) cannot be uniquely determined by the mixture fraction only, as can be seen in Fig. 3 a). Additional manifolds are therefore needed, for example, the progress variable and the enthalpy can be used to uniquely determine the temperature as seen in Fig. 3 b). These additional manifolds along with the non-monotonic behavior cause difficulties in retrieving data from the spray flamelet library.

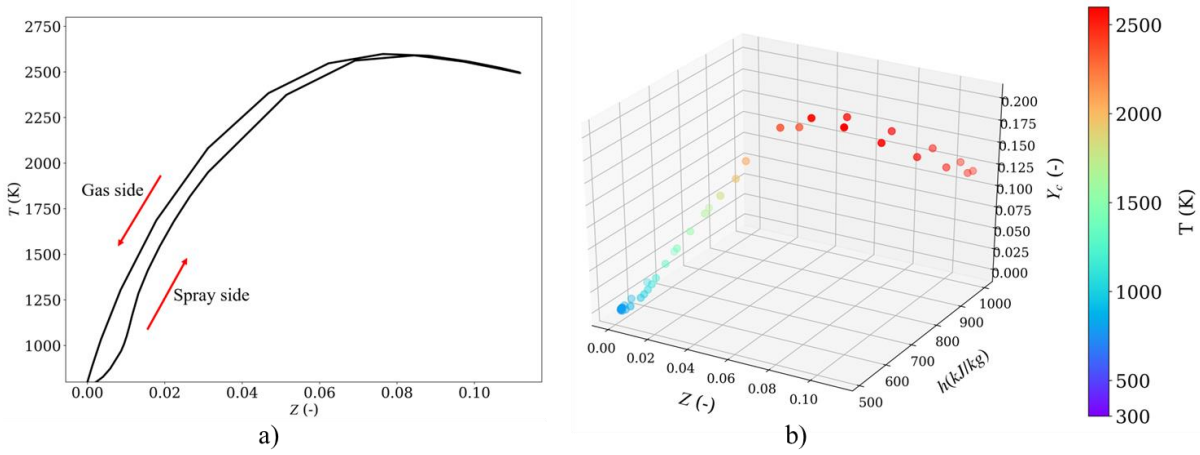

Fig. 3 Temperature profiles in the a) mixture fraction space and b) the Z-Y_c-h space.

IV. Turbulent Piloted Dilute Spray Combustion using the FGM approach

The spray flamelet results indicated that the mixture fraction no longer varies monotonically when the liquid fuel evaporation is incorporated, which causes some ambiguity in constructing look-up tables. Moreover, a typical spray flame library would require many parameters related to spray characteristics. Therefore, the gaseous diffusion flame configuration is used to build the look-up database to be coupled with a CFD solver. The presumed PDF approach was utilized to account for the turbulence-chemistry interaction. The preliminary goal was to implement the FGM approach for spray combustion studies. The piloted spray burner experimental data [9] was used for model validation. Detailed procedures are given as follows.

A. Descriptions of the piloted spray burner and numerical setup

To avoid uncertainties associated with liquid fuel atomization, the diluted spray anchored with piloted hot gas flow configuration as described in Ref. [9] was chosen. A multi-component kerosenes Jet-A surrogate fuel was used. Since the experimental data is not available for Jet-A fuel, a single component ethanol fuel case [9] was also included for the comparison. The CFD solver OpenFOAM [17] was used to couple with the FGM look-up table. For the experimental setup [9], the spray is generated by an ultrasonic nebulizer 215 mm upstream of the central fuel nozzle with a diameter D of 10.5 mm. In this study, the bulk velocity of the central jet, 60m/s, was not used as a fixed value for the inlet velocity profile. Instead, the experimental velocity data at the immediate downstream location ($x/D = 0.3$) of the jet exit was extracted as the inlet velocity profile. Both axial and radial velocity components corresponding to the experimental set B of EtF7 [9] were used. Other simulation boundary conditions for the central jet, pilot and the co-flow are listed in Table 1.

Table 1 Inlet conditions corresponding to the piloted spray burner [9]

Inlet conditions	U_{pilot} (m/s)	U_{coflow} (m/s)	$\dot{m}_{\text{carrier}}$ (g/s)	$\dot{m}_{\text{liquid}}$ (g/s)	$\dot{m}_{\text{vapor}}$ (g/s)	Z_{jet}
Value	11.5	4.5	376	60	5	0.013

A Lagrangian discrete method combined with a continuous Eulerian frame as implemented in the OpenFOAM was utilized to solve the two-phase combusting flow in conjunction with the pre-built FGM table. The computational domain covers the axial distance of 40D and 13.8D in the radial direction. The total cell number of the domain is 8000 with a refined mesh near the inlet and the centerline locations. The grid independence of the solution is ensured by the maximum deviation of temperature profiles less than 5% when compared with the 16000-cell mesh result. The statistically steady Favre-averaged governing equations were solved for the gas-phase with the standard $k-\varepsilon$ turbulence model by an implicit finite-volume method. The PIMPLE [17] algorithm was utilized for pressure-velocity fields. For the interactions between droplets and gas flow, there is a two-way coupling in mass and energy exchanges, while the exchange of momentum only takes place from the gas to liquid due to the dilute spray assumption. The Ranz-Marshall [18] correlation was applied to solve the mass/heat transfer coefficients. As to the spray parcels, the stochastic dispersion model due to the gas phase turbulence was employed, and only secondary breakup model TAB was modeled without primary breakup and coalescence. The chemical kinetics POLIMI_231 [14] consisted of 231 species and 5591 reactions was applied for Jet-A surrogate developed by our previous work [15], and the skeletal chemical-kinetic mechanism containing 31 species and 66 reactions [16] is used here to characterize the chemical reaction of ethanol.

The 1D non-premixed flamelet model is chosen as the basic flame structure to generate the flamelet library, which is accomplished by the open source solver Cantera [12]. A batch of steady laminar diffusion flamelet solutions was obtained covering a small mean strain rate to the maximum value corresponding to the extinction state.

For the FGM model, all thermal parameters are seen as the function of two controlling parameters: the mixture fraction Z and the reaction progress variable Y_C . The progress variable in this work is defined as the sum of the mass fractions of H_2O and CO_2, written as:

$$Y_C = Y_{H_2O} + Y_{CO_2} . \tag{2}$$

The definition of Y_C is not unique, other formulations [7, 19] have been used. After obtaining the solutions in the physical domain, the laminar flamelet was constructed in the $Z-Y_C$ space through post-processing the data.

For each 1D diffusion flame case, both fuel and air inlets are initialized with a temperature of 300 K at atmospheric pressure, and a heat source is provided to mimic the ignition process at the beginning. The distribution of temperature and progress variable source term $\dot{\omega}_{Y_C}$ for Jet-A and ethanol are illustrated in Fig. 4 and Fig. 5 in the two-dimensional $Z-Y_C$ map, respectively. It shows that, for a certain mixture fraction of the two fuels, the temperature increases as the reaction progresses, and the highest values of $\dot{\omega}_{Y_C}$ and temperature both fall in the region where the stoichiometric mixture fraction $Z_{st}=0.1$ for ethanol and $Z_{st}=0.068$ for Jet-A.

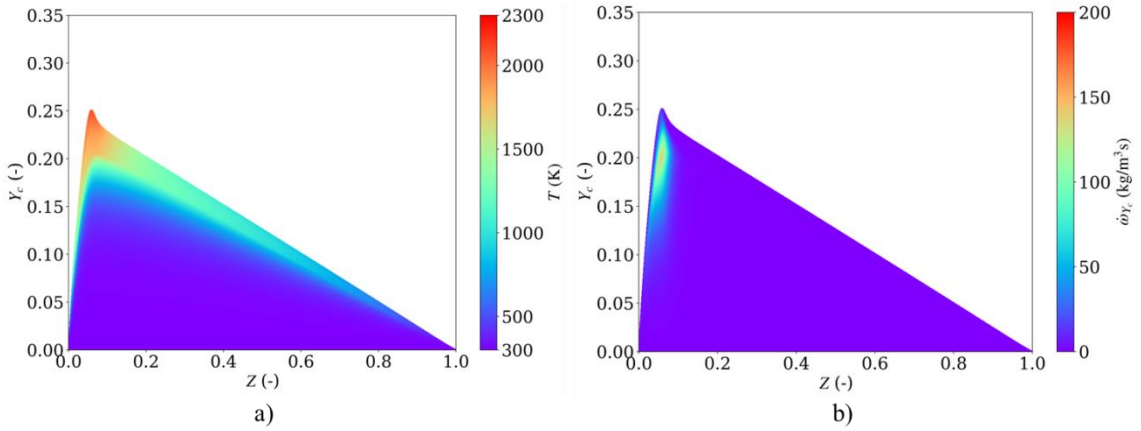

Fig. 4 The distribution of a) temperature and b) progress variable source term in the *Z*-Y_C map for Jet-A.

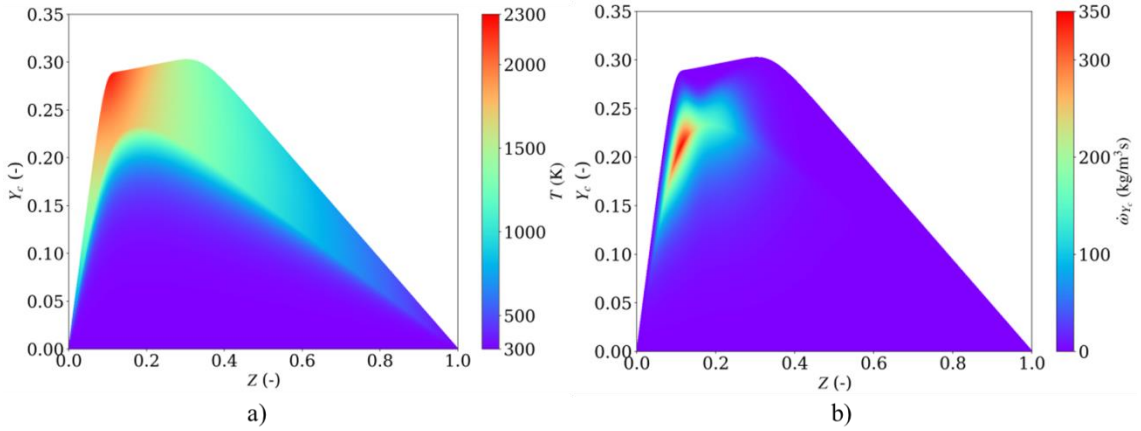

Fig. 5 The distribution of a) temperature and b) progress variable source term in the *Z*-Y_C map for ethanol.

For turbulent spray combustion, a joint PDF $\tilde{P}(Z,Y_C)$ (Probability Density Function) is introduced to account for the interaction of turbulence and combustion. Based on the widely used presumed PDF modeling [6, 19], the mixture fraction Z and the progress variable Y_C are assumed to be independent, that is, $\tilde{P}(Z,Y_C)=\tilde{P}(Z)\tilde{P}(Y_C)$. For the non-premixed flame, β-PDF and δ-PDF distributions are adopted for Z and C, respectively. Then the Favre-averaged scalar $\tilde{\phi}$ can be written in the form of

$$\tilde{\phi} = \int_0^1 \phi\left(Z, \tilde{Y}_C\right) \beta\left(Z; \tilde{Z}, Z''^2\right) dZ \,, \tag{3}$$

where $\beta\left(Z; \tilde{Z}, Z''^2\right)$ denotes the β-PDF. In this way, the tabulation scalar is then given by

$$\tilde{\phi} = \phi\left(\tilde{Z}, Z''^2, \tilde{Y}_C\right). \tag{4}$$

In the reactive two-phase flow, the filtered conservation equations of gas-phase continuity and momentum are given as

$$\frac{\partial \bar{\rho}}{\partial t} + \frac{\partial\left(\bar{\rho}\tilde{u}_i\right)}{\partial x_i} = \bar{\dot{S}}_v \,, \tag{5}$$

$$\frac{\partial\left(\bar{\rho}\tilde{u}_i\right)}{\partial t} + \frac{\partial\left(\bar{\rho}\tilde{u}_i\tilde{u}_j\right)}{\partial x_i} = -\frac{\partial \bar{p}}{\partial x_i} + \frac{\partial}{\partial x_j}\left(\bar{\tau}_{ij} - \overline{\rho u_i'' u_j''}\right) \tag{6}$$

In order to retrieve the tabulated parameters from the FGM library, filtered transport equations for mixture fraction and reaction progress variable are solved by

$$\left.\begin{aligned} \frac{\partial\left(\bar{\rho}\tilde{Z}\right)}{\partial t} + \frac{\partial\left(\bar{\rho}\tilde{u}_i\tilde{Z}\right)}{\partial x_i} &= \frac{\partial}{\partial x_j}\left[\bar{\rho}\left(\tilde{\alpha}_Z + \alpha_t\right)\frac{\partial \tilde{Z}}{\partial x_j}\right] + \tilde{S}_Z \\ \frac{\partial\left(\bar{\rho}\tilde{Y}_C\right)}{\partial t} + \frac{\partial\left(\bar{\rho}\tilde{u}_i\tilde{Y}_C\right)}{\partial x_i} &= \frac{\partial}{\partial x_j}\left[\bar{\rho}\left(\tilde{\alpha}_Z + \alpha_t\right)\frac{\partial \tilde{Y}_C}{\partial x_j}\right] + \bar{\dot{\omega}}_{Y_C} \end{aligned}\right\}, \tag{7}$$

where α_t is the turbulent diffusivity, $\tilde{S}_Z$ is a source term due to the spray evaporation, which can be modeled according to Baba et al. [20], i.e.,

$$\tilde{S}_Z = -\frac{1}{V_c}\sum_p \dot{m}_p N_p \,. \tag{8}$$

The chemical reaction source term $\bar{\dot{\omega}}_{Y_C}$ in Eq. (7) is calculated a priori in the 1D diffusion flame structure and stored in the tables.

According to Pera et al. [21], the transport equation of the variance of the mixture fraction is solved by

$$\frac{\partial\left(\bar{\rho}Z''^2\right)}{\partial t} + \frac{\partial\left(\bar{\rho}\tilde{u}_i Z''^2\right)}{\partial x_i} = \frac{\partial}{\partial x_j}\left[\bar{\rho}\left(\tilde{\alpha}_Z + \alpha_t\right)\frac{\partial Z''^2}{\partial x_j}\right] + 2\bar{\rho}\alpha_t\left(\frac{\partial \tilde{Z}}{\partial x_i}\right)^2 - 2\bar{\rho}\tilde{\chi} + \bar{\rho}\dot{W}^+ \,. \tag{9}$$

The standard *k*-ε model is adopted as the turbulence model when dealing with the turbulent viscosity in the above equations. The scalar dissipation rate $\tilde{\chi}$ is modeled by

$$\tilde{\chi} = C_\chi \frac{\varepsilon}{k} Z''^2 \,, \tag{10}$$

where C_χ is seen as a constant of 2.0. The evaporation source term $\bar{\rho}\dot{W}^+$ is closed as suggested by Rittler et al. [22], that is

$$\bar{\rho}\dot{W}^+ = \alpha Z''^2 \frac{\tilde{S}_Z}{\tilde{Z}} \,. \tag{11}$$

In which, a constant value of 0.5 is used for α .

B. Results and discussions

Fig. 6 shows the contour plots of the mean gas temperature of the EtF7 simulation results for both ethanol (upper half-domain) and Jet-A (lower half-domain). When the central spray jet develops downstream, the droplets start to evaporate due to the entrainment of surrounding hot pilot stream, and eventually lead to the establishment of the inner flame front at the axial location around $x/D=10$ for ethanol fuel. For Jet-A fuel, the flame front location moves further downstream since the volatility of the multi-component Jet-A fuel is much lower than the ethanol. It should be noted that the spray mass flow rates for Jet-A and ethanol are set to be the same. Since the mean molecular weight of Jet-A is about 3 times of ethanol, thus the droplet number of Jet-A fuel is much less than that of ethanol. This will result in a shorter liquid jet penetration of Jet-A as seen in Fig. 6.

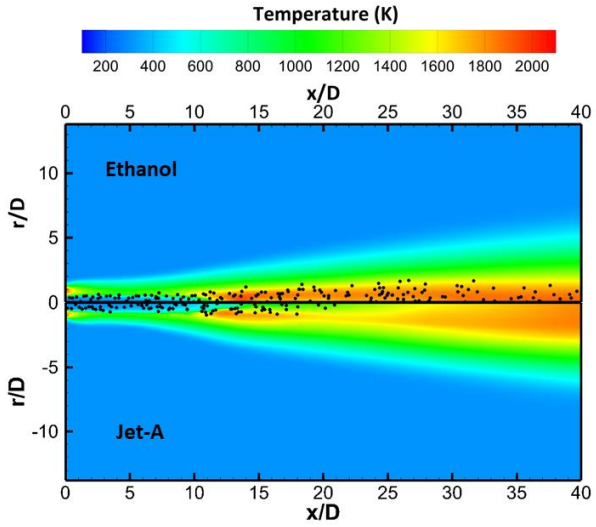

Fig. 6 Contours of the mean gas temperature for ethanol (upper) and Jet-A (lower). The black dots denote the penetration and positions of the spray parcels.

Fig. 7 shows the predicted SMD (Sauter Mean Diameter) radial profiles at four different axial locations. Since the experimental data for the kerosene fuel is not available, the ethanol spray combustion case results and experimental data [9] are plotted as a reference. Overall, the predicted SMD profiles in the ethanol cases are consistent and are in good agreement with the experimental data, especially at locations $x/D=5$ and $x/D=10$. At further downstream locations (e.g. $x/D=20$), the simulation shows an under-prediction of the SMD distribution, which can be attributed to the corresponding over-predicted temperature profile seen as Fig. 6. The higher gas temperature near the central line in that region enhances the evaporation of the droplets, thus leads to smaller droplet size. For the Jet-A case, the predicted SMD distributions are similar to the ethanol case, except at location $x/D=20$ where the SMD of Jet-A is much smaller than that of ethanol. As indicated previously, a less amount of Jet-A droplets was injected at the inlet location, thus the Jet-A droplets evaporate more quickly, corresponding to the parcel distributions in Fig. 6.

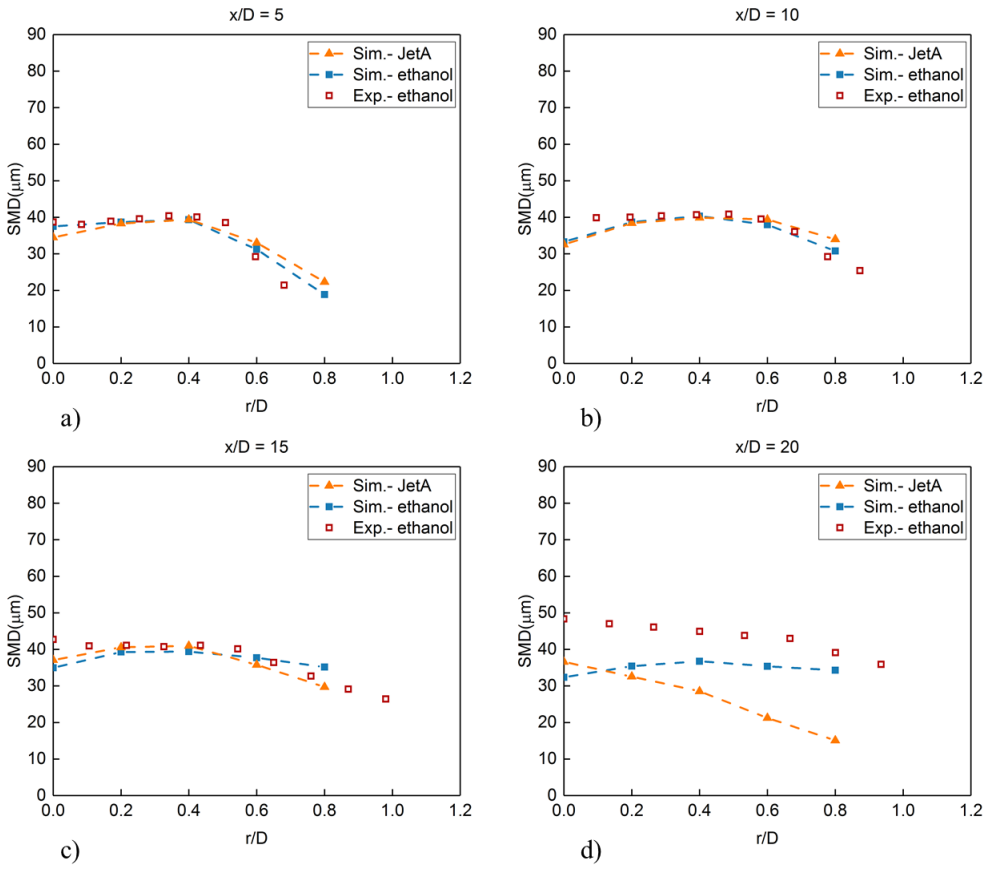

Fig. 7 Predicted SMD radial profiles at axial locations a) *x*/*D*=5, b) *x*/*D*=10, c) *x*/*D*=15 and d) *x*/*D*=20 for both ethanol and Jet-A in comparison with experimental data; data for ethanol only.

The mean profiles of the predicted gas temperature are displayed at three different downstream locations in Fig. 8 for both Jet-A and ethanol fuels. Except for the near spray jet region for the ethanol case, the calculated gas temperature field is higher than the experimental data. The discrepancy of the temperature profiles is likely attributed to the original construction of the laminar flamelet table. It should be noted that the FGM table used in this case is adiabatic, which lacks the non-adiabatic effect of the droplet evaporation. Consequently, the temperature field was overall overestimated by the current FGM table without properly considering the enthalpy loss.

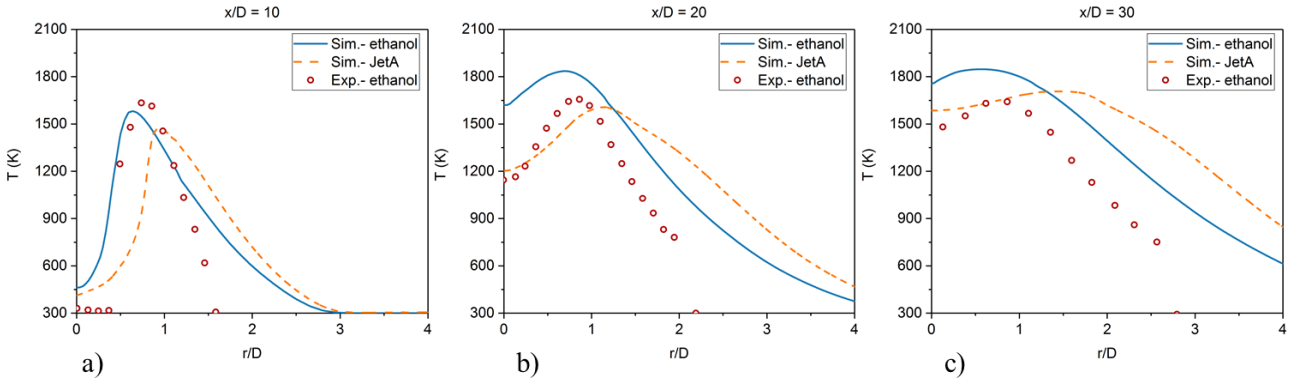

Fig. 8 Predicted mean gas temperature profiles at a) *x*/*D*=10, b) *x*/*D*=20 and c) *x*/*D*=30 for both ethanol and Jet-A in comparison with experimental data of ethanol; data for ethanol only.

The enthalpy loss due to the droplet evaporation can be considered by solving the enthalpy equation as an additional manifold in the tabulation process [6, 11]. The solutions are tabulated at different initial absolute enthalpy levels and can be achieved by changing both-side inlet temperatures at the same time as the 1D diffusion flame structure from 200 K to 300 K by the interval of 20 K. In order to assess the results given by the FGM approach involving 3 controlling variables (mixture fraction Z, progress variable Y_C and absolute enthalpy h_a), a benchmark problem was set up for comparison. To this end, a two-dimensional laminar counterflow spray flame structure solution was obtained by solving all governing equations, with direct integrations of finite-rate chemical reactions, by the OpenFOAM CDF code. This solution would serve as a "DNS" result and be compared to the solution obtained by CFD/FGM coupling.

For the 2D counterflow configuration, a square mesh with 80×80 nodes, corresponding to a $20\text{mm}\times20\text{mm}$ physical domain was used. The spray parcels with a uniform droplet diameter 40μm were injected from the upper-side inlet, and there is no slip velocity between the droplet and air flow at the spray inlet. An ignition source is activated for several time steps to generate the flame front, and Fig. 9 shows the final steady flame structure in terms of temperature for the "DNS" approaches.

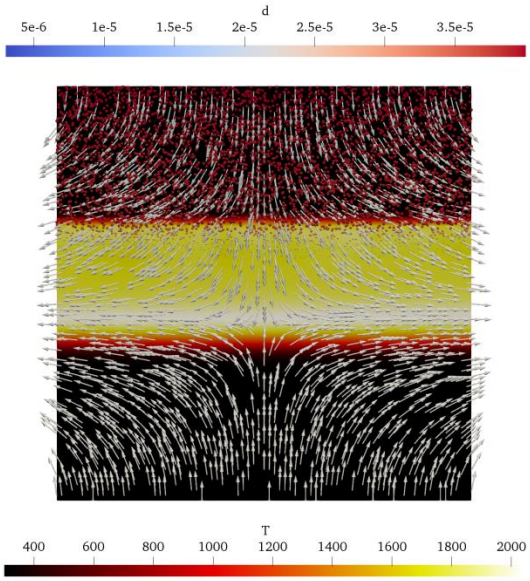

Fig. 9 Temperature map of the steady spray (represented by dots) flame structure using the "DNS" approach (the upper and lower inlet velocities are 1m/s and -1m/s, respectively, and the temperature of both inlets are 300 K).

The profiles of temperature and mass fractions of CO and CO2 at the central line are shown in Fig. 10. To further validate the effect of the absolute enthalpy h_a, a 2-variable manifold (mixture fraction and progress variable) is employed, denoted by the red solid line. Apparently, the temperature field calculated by the 2-variable FGM is over-predicted, which can be accounted for due to the lack of evaporation effect in the flamelet database. Using the 3-variable FGM, this overprediction has been improved at the first temperature peak, while the improvement for the second peak is not quite obvious. The cause of the phenomenon could be attributed to the evaporation source distribution in the physical domain. Most of the evaporation process occurs around the location of the first temperature peak, leading to a low absolute enthalpy level. Hence, the evaporation effect would decrease the temperature field by using the 3-variable FGM, as compared with the 2-variable FGM. However, the majority of droplets cannot reach the location of the second temperature peak, indicating that the temperature field reduction would be limited with the 3-variable FGM approach. From this comparison, it can be concluded that the non-adiabatic effect of evaporation does play a significant role and can be captured by the 3-variable FGM tabulation.

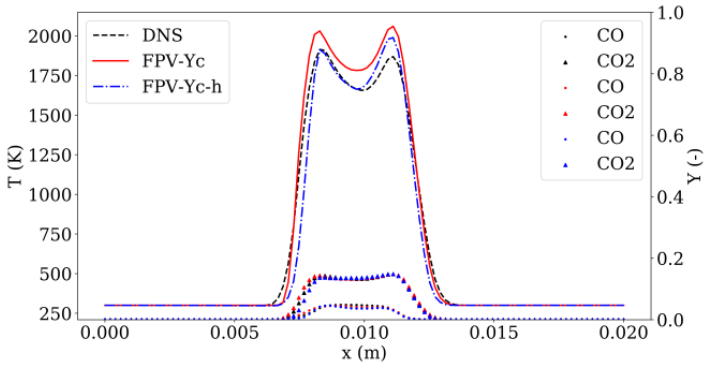

Fig. 10 The temperature and CO/CO_2 profiles at the central line for three simulation results, where "DNS" denotes temperature of the direct integration of chemical reaction, "FPV-Yc" and "FPV-Yc-h" are gaseous FGM approach without and with enthalpy manifold, respectively.

V. Conclusion

In this study, the partially-premixed combustion regime has been investigated in a one-dimensional counterflow spray diffusion flame configuration. The results uncover the intrinsic difference in comparison with the corresponding gaseous diffusion flame. However, due to the non-monotonicity of the mixture fraction, the resulting spray flame FGM tabulation was not implemented into a CFD solver in the current study. A multi-component Jet-A surrogate gaseous FGM tabulation was used to predict the turbulent piloted dilute spray combustion in which the two-way coupling Eulerian-Lagrangian calculation frame was used. A presumed PDF is utilized in the FGM tables to account for the interaction between turbulence and chemistry. The numerical results for both kerosene fuel and ethanol fuel show a good agreement with experimental data in terms of SMD distribution, while the temperature field is over-predicted as a whole. The cause of the deviation was investigated further by adding the absolute enthalpy as an extra variable to the FGM tables using a 2-dimensional counterflow configuration as a benchmark case. The comparison among the 2-variable FGM, 3-variable FGM and the full spray flame simulation indicated that adding the enthalpy variable to the FGM can capture the non-adiabatic process of droplet evaporation of the FGM approach.

Future work will continue in establishing spray flamelet database, mainly to address the issue of table look-up process due to non-monotonic variation of mixture fraction. Experimental database for multi-component spray combustion is highly needed.

Acknowledgment

This work was partially supported by the National Science Foundation of China (NSFC) under grant number 91741111.

References

[1] Yang, T., Wang, Q., Yi, R., and Chen, C. P. "Modeling Spray Combustion of Jet-A in a Constant-Volume Combustion Chamber," *AIAA Propulsion and Energy Forum and Exposition*, Cincinnati, OH, 2018. doi: 10.2514/6.2018-4565

[2] Pierce, C. D., and Moin, P,. "Progress-variable approach for large-eddy simulation of non-premixed turbulent combustion," *Journal of Fluid Mechanics*,Vol. 504, No. 504, 2010, pp. 73-97. doi: 10.1017/S0022112004008213

[3] Watanabe, H., Kurose, R. and Hwang, S.-M., "Characteristics of flamelets in spray flames formed in a laminar counterflow," *Combustion and Flame*, Vol. 148, No. 4, 2007, pp. 234-248. doi: 10.1016/j.combustflame.2006.09.006

[4] Franzelli, B., Fiorina, B., and Darabiha, N., "A tabulated chemistry method for spray combustion," *Proceedings of the Combustion Institute*, Vol. 34, No. 1, 2013, pp. 1659-1666. doi: 10.1016/j.proci.2012.06.013

[5] Hollmann, C. and Gutheil, E., "Diffusion Flames Based on a Laminar Spray Flame Library," *Combustion Science and Technology*, Vol. 135, No. 1-6, 1998, pp. 175-192.

doi: 10.1080/00102209808924156
[6] El-Asrag, H. A., Braun, M. and Masri, A. R., "Large eddy simulations of partially premixed ethanol dilute spray flames using the flamelet generated manifold model," *Combustion Theory and Modelling*, Vol. 20, No. 4, 2016, pp. 1-25. doi: 10.1080/13647830.2016.1159732
[7] Hu, Y., Olguin, H. and Gutheil, E., "A spray flamelet/progress variable approach combined with a transported joint PDF model for turbulent spray flames," *Combustion Theory and Modelling*, Vol. 21, No. 3, 2017, pp. 1-28. doi: 10.1080/13647830.2016.1277589
[8] Hu, Y. and Kurose, R., "Nonpremixed and premixed flamelets LES of partially premixed spray flames using a two-phase transport equation of progress variable," *Combustion and Flame*, Vol. 188, 2018, pp. 227-242. doi: 10.1016/j.combustflame.2017.10.004
[9] Gounder, J. D. and Kourmatzis, A., "Turbulent piloted dilute spray flames: Flow fields and droplet dynamics," *Combustion and flame*,Vol. 159, No. 11, 2012, pp. 3372-3397. doi: 10.1016/j.combustflame.2012.07.014
[10] Kee, R. J., Coltrin, M. E. and Glarborg, P. *Chemically Reacting Flow: Theory and Practice*, John Wiley & Sons, 2005.
[11] Luo, Y., Wen, X., Wang, H., Luo, K. and Fan, J., "Evaluation of different flamelet tabulation methods for laminar spray combustion," *Physics of Fluids*, Vol. 30, No. 5, 2018, p. 053603. doi: 10.1063/1.5026739
[12] Goodwin, D. G., Moffat, H. K. and Speth, R. L., "Cantera: An object-oriented software toolkit for chemical kinetics, thermodynamics, and transport processes.", Pasadena, CA. Version 2.4.0, 2009.
[13] Miller, R. S., Harstad, K. and Bellant, J., "Evaluation of equilibrium and non-equilibrium evaporation models for many-droplet gas-liquid flow simulations," *Journal of Multiphase Flow* Vol. 24, No. 6, 1998, pp. 1025-1055. doi: 10.1016/S0301-9322(98)00028-7
[14] Ranzi, E., Frassoldati, A., Stagni, A., Pelucchi, M., Cuoci, A. and Faravelli, T., "Reduced Kinetic Schemes of Complex Reaction Systems: Fossil and Biomass-Derived Transportation Fuels,"*International Journal of Chemical Kinetics*, Vol. 46, No. 9, 2014, pp. 512–542. doi: 10.1002/kin.20867
[15] Chen, X., Khani, E. and Chen, C. P., "A unified jet fuel surrogate for droplet evaporation and ignition," *Fuel*, Vol. 182, 2016, pp. 284-291. doi: 10.1016/j.fuel.2016.05.114
[16] Millán-Merino, A., Fernández-Tarrazo, E., Sánchez-Sanz, M. and Williams, F. A., "A multipurpose reduced mechanism for ethanol combustion," *Combustion and Flame*, Vol. 193, 2018, pp. 112-122. doi: 10.1016/j.combustflame.2018.03.005
[17] Weller, H. G., Tabor, G., Jasak, H. and Fureby, C, "A tensorial approach to computational continuum mechanics using object-oriented techniques," *Computers in Physics*, Vol. 12, No. 6, 1998, pp. 620-631. doi: 10.1063/1.168744
[18] Ranz, W. and Marshall, W. R., "Evaporation from drops," *Chem. eng. prog*, Vol. 48, No. 3, 1952, pp. 141-146.
[19] Ma, L., Naud, B. and Roekaerts, D., "Transported PDF Modeling of Ethanol Spray in Hot-Diluted Coflow Flame," *Turbulence and Combustion*, Vol. 96, No. 2, 2016, pp. 469-502. doi: 10.1007/s10494-015-9623-3
[20] Baba, Y. and Kurose, R. J., "Analysis and flamelet modelling for spray combustion," *Journal of Fluid Mechanics*, Vol. 612, No. 612, 2008, pp. 45-79. doi: 10.1017/S0022112008002620
[21] Pera, C., Réveillon and J., Vervisch, L., "Modeling subgrid scale mixture fraction variance in LES of evaporating spray," *Combustion and Flame*, Vol. 146, No. 4, 2006, pp. 635-648. doi: 10.1016/j.combustflame.2006.07.003
[22] Rittler, A., Proch, F. and Kempf, A. M., "LES of the Sydney piloted spray flame series with the PFGM/ATF approach and different sub-filter models," *Combustion and Flame*, Vol. 162, No. 4, 2015, pp. 1575-1598. doi: 10.1016/j.combustflame.2014.11.025